# Improved strain measuring using fast strain-encoded cardiac MR

# IMPROVED STRAIN MEASURING USING FAST STRAIN-ENCODED CARDIAC MR

*Abdallah G. Motaal* [1] †, *Nael F. Osman* [1,2]

[1] Medical Imaging and Image Processing Lab, Center for Informatics Sciences, Nile University, Egypt
[2] Radiology Department, School of Medicine, Johns Hopkins University, Baltimore, MD, USA

## ABSTRACT

The strain encoding (SENC) technique encodes regional strain of the heart into the acquired MR images and produces two images with two different tunings so that longitudinal strain, on the short-axis view, or circumferential strain on the long-axis view, are measured. Interleaving acquisition is used to shorten the acquisition time of the two tuned images by 50%, but it suffers from errors in the strain calculations due to inter-tunings motion of the heart, which is the motion between two successive acquisitions. In this work, a method is proposed to correct for the inter-tunings motion by estimating the motion-induced shift in the spatial frequency of the encoding pattern, which depends on the strain rate. Numerical data is generated to test the proposed method and real images of human subjects are used for validation The results show an improvement in strain calculations so as to relax the imaging constraints on spatial and temporal resolutions and improve image quality.

***Index Terms—*** Cardiac magnetic resonance imaging, strain encoding, tissue deformation, interleaving acquisition.

## 1. INTRODUCTION

MRI is the only imaging modality capable of directly imaging the motion inside the heart [1–5]. MR tagging is capable of noninvasive and accurate measurements of myocardial motion. MR tagging uses special pulse sequences at end-diastole to create planes of saturated magnetization that are traditionally oriented orthogonal to the image plane [1, 3-4]. These tag surfaces bend with the deformation of the myocardium and their intersections with the image planes deform from straight lines into bent curves. Detailed motion of the myocardium can be deduced by analyzing the deformation of the tag lines found within these images [6, 7]. Recently Strain Encoded MRI (SENC) is used for direct encoding of regional strain into the acquired image [8]. SENC is used to measure the strain in the direction orthogonal to the imaging plane, so it can be used in quantifying regional function of heart. The imaging principle is based on MR tagging, but in contrast to usual techniques, tag planes are initially oriented parallel to the imaging plane. The data processing principle is based on analyzing the spectral peaks in *k*-space that are created by the tagging process [8-10]. It turns out that by acquiring two images with different *z* phase encodes, where the *z* direction is the slice select direction, a dense estimate of longitudinal strain on the short-axis image plane can be calculated. As two images with different *z* phase encodes are acquired to get the full strain map, so, the two images must be acquired at the same instant of time to give an accurate strain estimation. Non-interleaving acquisition is used, where it gives an accurate estimate of the strain values; however, it is time consuming, as two sets of images, low-tune and high-tune images, are acquired at different tuning values for every time frame. Recently, fast-SENC (*f*-SENC) is proposed [11], where an interleaving acquisition is used. Consequently, a single set of images is acquired by alternating the tunings throughout the time-frames, and as a result, the acquisition time is reduced by half. This technique leads to errors in the strain calculation due to the inter-tuning motion of the heart. In this work we represent a method to correct the measured strain values that arise in case of using low-temporal resolution interleaving acquisition. The technique is validated using numerical simulations and real data of normal volunteers. In the following sections we show a brief background and describe the approach, show how it is implemented, and analyze trade-offs in performance as a function of image acquisition parameters.

## 2. THEORY

### 2.1. Strain Encoded MRI

The SENC technique was introduced to measure the local strain distribution of deforming tissues directly and without the need for sophisticated post-processing as in MR tagging. In SENC MRI, the magnetization of the object under test at location (x, y) is modulated in the slice-selection direction with a sinusoidal pattern of a spatial frequency, $\omega_0(x, y)$ which is initially uniform everywhere. Because of the motion of the LV, myocardial displacement and deformation occurs, and the tag pattern moves and undergoes deformation that makes the tissue's new frequency $\omega(x, y)$

† Currently, BioMedical Image Analysis, and Biomedical Nuclear Magnetic Resonance Research Labs, Biomedical Engineering Department, Eindhoven University of Technology, Netherlands. (*a.motaal@tue.nl*)

proportionally changing with the degree of deformation at the location (x, y). Figure 1 shows the frequency component in the *z*-direction for a voxel having no strain and being contracted.

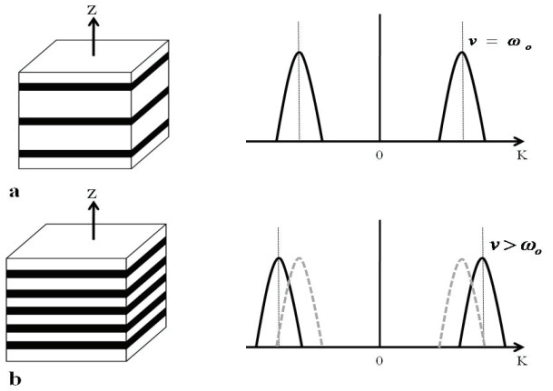


Figure 1. Magnetization pattern inside a voxel and its corresponding frequency component during a) relaxation and b) contraction

The signal intensity at a certain location (x, y) can be given by [8]

$$I(x, y) = \rho(x, y)\ S(\omega_T - \Omega(x, y)), \qquad (1)$$

where ρ(x, y) represents the proton density of the voxel; S(ω) is the Fourier transform of the slice profile—which is determined by the envelope of the applied slice selection RF pulse; $\omega_T$ is the tuning frequency, which is determined during the image acquisition by an applied tuning gradient, and Ω is the local frequency. The function S(.) is shifted in proportion to the change in the local frequency, Ω, which depends on the tissue deformation. Therefore, measuring the frequency allows the estimation of the tissue strain. The central frequency of the slice can be given by [8]:

$$\mu(x, y) = \frac{\omega_A\, |I(x, y; \omega_A)| + \omega_B\, |I(x, y; \omega_B)|}{|I(x, y; \omega_A)| + |I(x, y; \omega_B)|}, \qquad (2)$$

where $\omega_A$, $\omega_B$ are the low- and high-tuning frequencies, respectively. Thus the strain at (x, y) can be given by [8]

$$\varepsilon(x, y) = \left(\frac{\omega_O}{\mu(x, y)} - 1\right) \times 100 \qquad (3)$$

### 2.2. Non-Interleaving Acquisition

Originally, two images are required at the same instant of time with two different tuning frequencies in order to estimate the strain. This is done by repeating the acquisition, which leads to doubling of the acquisition time. Figure 2 shows a non-interleaving acquisition.

Consider the slice profile in the frequency domain is as shown in Figure 3, where it is represented by a *sinc* profile [8]. By acquiring signals at two different tunings, $\omega_L$ and $\omega_H$, we seek to determine the frequency center of the slice profile. Table 1 shows the low- and high-tune images acquired at different time-frames. The two images correspond always to the same points in time in the cardiac cycle, which means that the slice profile is at the same location when acquiring the low- and high-tune images. Because of the contraction of the slice, the spatial frequency of the tag pattern increases and the slice profile shifts to a higher frequency, and the low- and high-tune images are acquired, and the process is repeated over the acquisition time.

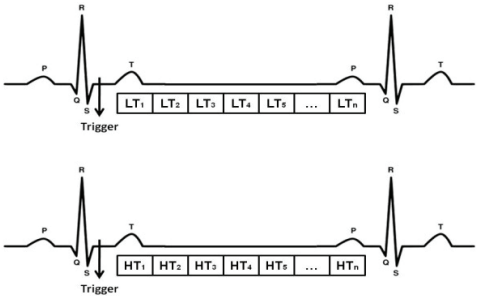


Figure 2. Original, non-interleaving acquisition: Two sets are acquired in separate breath holds for two different tunings.

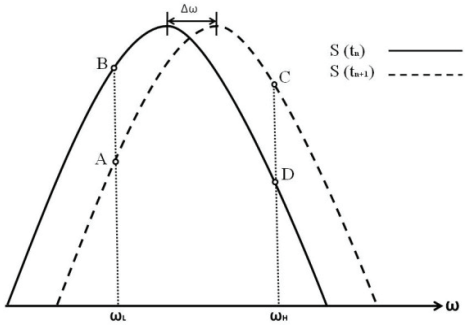


Figure 3. The slice profile in the frequency domain at $t_n$ and $t_{n+1}$

Table 1. Low- and high-tune images at two time frames $t_n$ and $t_{n+1}$

| | $t_n$ | $t_{n+1}$ |
|---|---|---|
| Low-Tune | **B** | **A** |
| High-Tune | **D** | **C** |

### 2.3. Interleaving Acquisition

By using interleaving acquisition [11], a single set of images, *I*, is acquired by alternating the tunings throughout the time-frames (i.e. a low-tune image is acquired, followed by a high-tune image and this is repeated over the acquisition time, as shown in Figure 4). The acquired dataset, *I*, can be described as:

$$I = \left\{ I_n \right\}_{n=1}^{N}$$

where, $I_n$ is $\begin{cases} \text{Low tune image} & \text{n is odd} \\ \text{High tune image} & \text{n is even} \end{cases}$

and for each image, the pixel intensity at certain location (x, y) can be represented as shown in equation (1)

$$I_n(x, y) = \rho(y, t)\, S(\omega(n) - \Omega_n(x, y)) \qquad (4)$$

where , $\omega(n) = \begin{cases} \omega_{LT} & \text{n is odd} \\ \omega_{HT} & \text{n is even} \end{cases}$

The strain maps are then constructed from every two successive images as shown in Figure 5. Therefore, no need to double the acquisition time; however, at the expense of introducing errors in determining the local frequencies of the slice for low temporal resolution sequences.

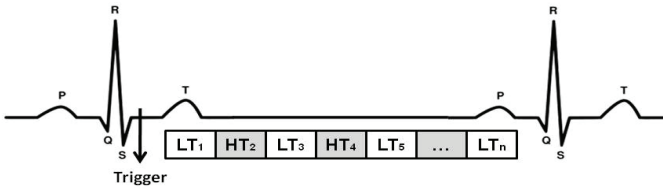


Figure 4. Interleaved acquisition of SENC, where the odd time-frames are encoded with low tuning and the even time-frames with high tunings.

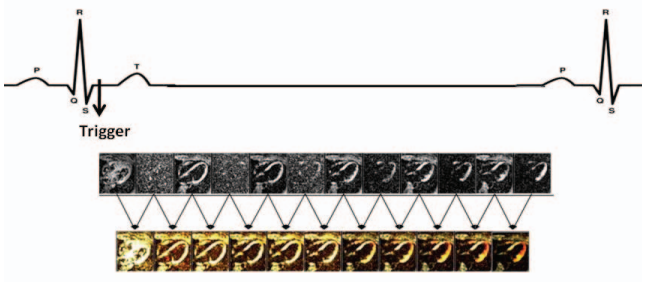


Figure 5. The functional images are constructed from every two successive images in the acquired sequence

As each strain map, Sn, is constructed from every two successive images, so the resultant strain maps will be N-1 time frames, where they can be calculated using the following equations:

$$\Omega_n = \frac{\omega(n)\, I_n + \omega(n+1)\, I_{n+1}}{I_n + I_{n+1}}, \quad n = 1,...,N-1 \qquad (5)$$

$$S_n = \left(\frac{\omega_o}{\Omega_n} - 1\right) \times 100, \quad n = 1,...,N-1 \qquad (6)$$

### 2.4. Interleaving Base Error in Strain Measurements

At low temporal resolution, the low- and high-tune images will correspond always to different points in time in the cardiac cycle. For example, when the two signals are acquired during the contraction of the heart, they will correspond to different shifts in frequency. Because these two tunings do not correspond to the same peak, the measured strain will be over- or under-estimated based on the order of the tunings. To correct this error, high temporal resolution may be used, however; it is very challenging and constrained. Figure 6 shows the error arises in case of using interleaving acquisition, where simulated SENC images are generated with low temporal resolutions.

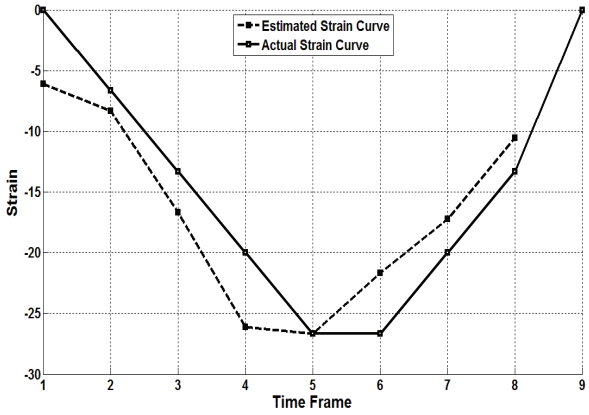


Figure 6. Ideal and Estimated Strain Curves in a low temporal resolution simulated SENC sequence

### 2.5. Correction of Interleaving Error

In original interleaving acquisition SENC computation, the local frequency in each time frame is computed from the low- and high-tune images using equation 5. After estimating the local frequency, the strain is calculated using equation 6. Figure 7 shows the block diagram of original *f*-SENC computation.

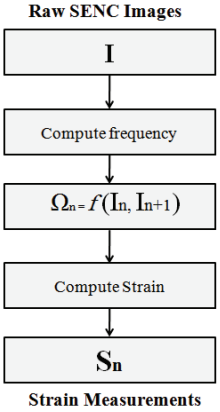


Figure 7. Original f-SENC Computation

In this work, a technique is proposed to correct for the inter-acquisitions misalignment by estimating the shift in the frequency, and then use that to re-estimate the frequency shift. This is repeated until the algorithm converges to a final solution—presumably close to the real frequency shifts.

It can be observed that the error arising in the interleaving acquisition is due to the wrong value of one of the two acquired signals. Therefore, if the wrong signal is corrected, the actual local frequency can be calculated. In Figure 3 for the timeframe $t_n$, the value of the high-tune image using non-interleaving method is *D*, which is the actual correct value, but in case of interleaving method it is *C*, a wrong value.

By estimating the value *D* from *C*, we can estimate the actual local frequency. In figure 8, it is noticed that *D* can be mapped from *C* through the following relation:

$$D = \mathrm{Sinc}\,(\mathrm{Sinc}^{-1}(C) + \Delta\omega), \qquad (7)$$

where $\Delta\omega$ is the shift in the frequency between the two acquisitions, and $Sinc^{-1}$ can be defined in the period $[-\pi, \pi)$

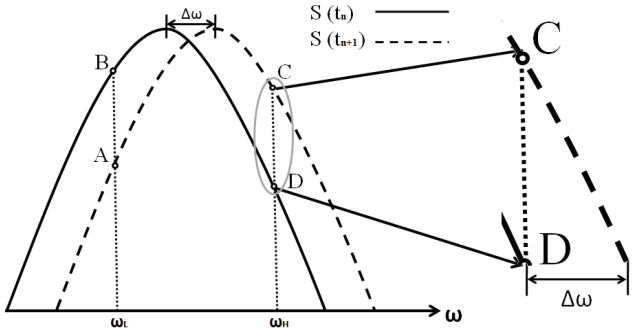


Figure 8. The slice profile in the frequency domain at $t_n$ and $t_{n+1}$

By knowing the $\Delta\omega$, the signal intensity can be corrected. In order to get the $\Delta\omega$, however, we initially calculate the local frequencies using the original *f*-SENC computations. Then from these initial estimates, $\Omega$, an approximate estimation of the change in the frequency, $\Delta\omega$, is estimated.

The new signals computed at all the timeframes, *I'*, are then used to correct for the frequency shifts between the time frames. The estimated frequencies are not necessarily the correct ones, thus, the correction algorithm is repeated until converging to the actual frequency shifts, and finally, the strain maps is constructed. In general, the updated time frame is a function of the original time frame and the change in the frequency, $\Delta\omega$, which can be represented by:

$$I_n^{'} = f\,(I_n, \Omega_{n+1} - \Omega_n)$$

In other words, the general correction function is:

$$I^{'} = Sinc\ (Sinc^{-1}(I) + \Delta\omega), \qquad (8)$$

Figure 9 shows a block diagram of the proposed algorithm. The first step in the algorithm is calculating the local frequencies using original *f*-SENC computation, i.e. $\Delta\omega$s are zeros, and then, initial values for the change in the frequency are estimated. The raw SENC images and the $\Delta\omega$s are fed into the correction function to get an updated SENC images using equation 8, and this cycle is repeated where the local frequencies, $\Omega$, are converging until reaching the final values that are then used to compute the strain measurements.

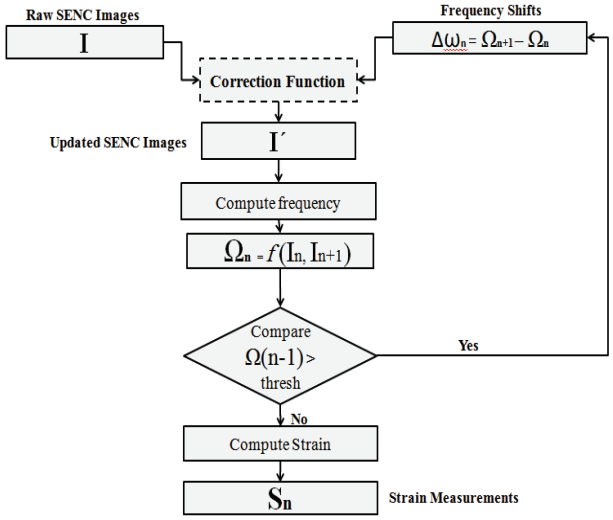


Figure 9. A block diagram showing the proposed correction algorithm

## 3. EXPERIMENTS

### 3.1. Numerical Experiments

In order to validate the proposed method, numerical simulations are used to generate SENC images with the two different acquisition methods for comparison with the ground truth measurements of the strain. The imaging parameters were as follows: slice thickness = 10 mm, $\omega_0$ = 0.21 $mm^{-1}$, $\omega_L$ = 0.2 $mm^{-1}$ and $\omega_H$ = 0.3 $mm^{-1}$, where the low- and high-tune frequencies correspond to max strain = +5 (stretching) and minimum strain = -30 (contraction), respectively. The simulated strain changed linearly with time.

To investigate the dependence of the proposed method on the rate of change of the local frequencies, seven data sets representing SENC images with different rates of change in strain were generated and used in the experiment.

We are also interested in examining the performance of the algorithm with different temporal resolutions. The seven datasets were generated at three temporal resolutions: 32, 52 and 88 milliseconds, which correspond to 25, 15 and 9 frames per cardiac cycle, respectively. It is expected that the error increases by decreasing the temporal resolution.

### 3.2. Real Data

The algorithm was also tested on real SENC images obtained from Philips Achievea MRI scanner (Philips Health Care). Images were obtained for a normal subject after his consent on an Institutional Review Board (IRB)-approved form. Two SENC sequences were obtained: interleaving and non-interleaving SENC sequences. The non-interleaving dataset provides the actual strain curve. Comparison was done between the strain curves using the interleaving acquisition before and after correction, and the curve resulted from the non-interleaving SENC sequence.
In order to assess the improvement in measuring strain of the proposed method, the root-mean square-error, RMSe, between the simulated strain curve, exact curve, and the curve before and after correction are measured.

## 4. RESULTS

### 4.1. Simulated Images

Figure 10 shows a simulated low- and high-tune SENC image at the beginning of the cardiac cycle. The images consist of two concentric annuli where the inner one is contracting with maximum strain values 0, -5… -30 for seven different datasets, respectively, and change linearly with time. The outer annulus represents the static tissue with a constant zero strain throughout the cardiac cycle.

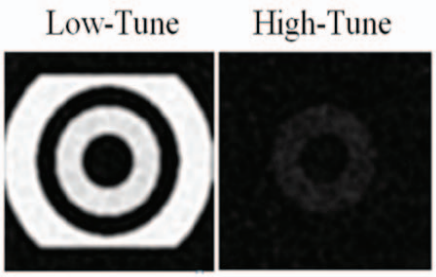


Figure 10. Simulated low- and high-tune images at end diastole

Figure 11 shows the strain curve without applying the correction algorithm compared to the ideal strain curve. It is noticed that there is an error, and this is due to the interleaving acquisition, although high temporal resolution is used. Also, this error increases as the temporal resolution degrades.
Fig. 12 shows the result after applying the correction algorithm. As expected from the Theory section, the measured strain curve is corrected and become nearly identical to the ideal strain curve. Figure 13 shows the root-mean-square error before and after applying the correction algorithm in the seven datasets for the three different temporal resolutions. As it can be noticed the root-mean-square error is inversely proportional with the temporal resolution, while directly proportion with the strain rate.

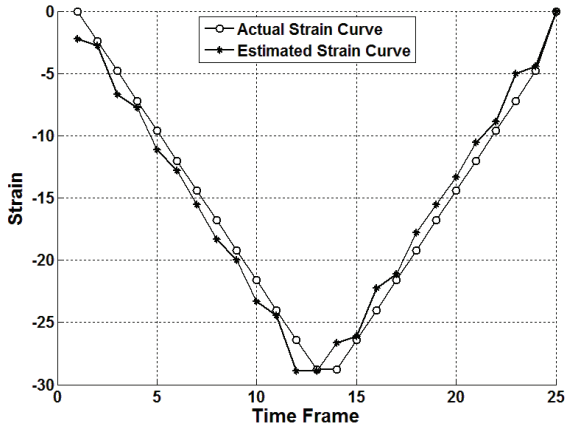


Figure 11. The exact and estimated strain curves before applying the correction algorithm on a simulated SENC sequence

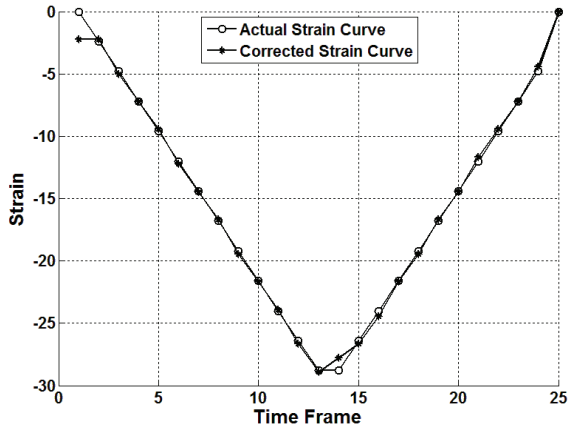


Figure 12. The exact and corrected strain curves after applying the correction algorithm on a simulated SENC sequence

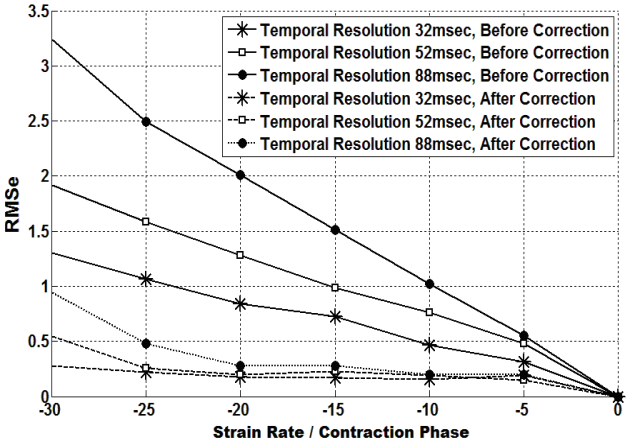


Figure13. The root-mean-square error between the exact and the measured strain values before and after correction for the seven datasets at the three different temporal resolutions

### 4.2 Real Images

Real data is used to validate the proposed method. Figure 14 shows low- and high-tune images at end-diastole and end-systole for non-interleaving SENC sequence.

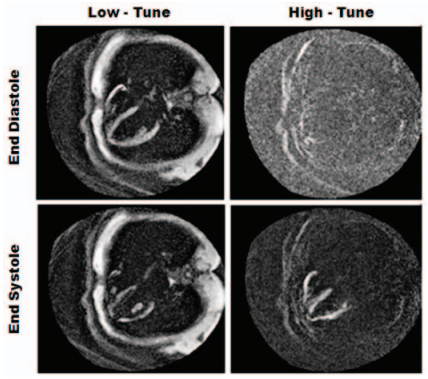


Figure 14. low- and high-tune SENC images at end-systole and end-diastole

Interleaving acquisition sequences are acquired using different temporal resolutions and the RMSe between the estimated strain curves and the actual strain curve is calculated. The correction algorithm is applied on the different datasets, and the RMSe for all the datasets decreased, as expected. Figure 15 shows the RMSe after applying the correction algorithm for a sequence with a temporal resolution 114.2 msec.

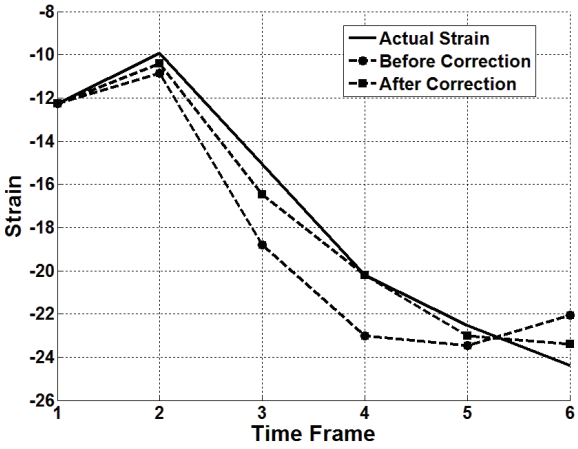


Figure 15. The actual strain curve and strain curves before and after correction for a real MR data.

## 5. DISCUSSION AND CONCLUSION

The proposed correction algorithm shows improvements in the strain measurements and better performance compared to a former method shown in [12] that was assuming a triangular slice profile in the frequency domain. As an example, applying the former method on a dataset with a temporal resolution 114.2 msec, the RMSe is decreased from 2.1971 to 1.032, while using the method proposed in this work, the RMSe decreased to 0.901.

In conclusion, a method is proposed for correcting the error in strain measurements due to inter frame motion in interleaving SENC acquisition. The method is able to correct the errors in strain calculations, and the corrected curves would allow for better analysis of the heart condition. The correction algorithm is more tolerant of lower temporal resolution, which is suitable for faster acquisition of SENC images with wider temporal separation, and this leads to improvement in the image quality and increase in the SNR.

## REFERENCES

[1] Zerhouni EA, Parish DM, Rogers WJ, Yang A, Shapiro EP. Human heart: tagging with MR imaging—a method for noninvasive assessment of myocardial motion. Radiology 1988;169:59–63.

[2] Pelc NJ, Herfkens RJ, Shimakawa A, Enzmann D. Phase contrast cine magnetic resonance imaging. Magn Reson Q 1991;7:229–254.

[3] Axel L, Dougherty L. MR imaging of motion with spatial modulation of magnetization. Radiology 1989;171:841–845.

[4] Axel L, Dougherty L. Heart wall motion: improved method of spatial modulation of magnetization for MR imaging. Radiology 1989;172:349.

[5] McVeigh ER. Regional myocardial function. Cardiol Clin 1998;16:189– 206.

[6] McVeigh ER, Zerhouni EA. Noninvasive measurement of transmural gradients in myocardial strain with MR imaging. Radiology 1991;180: 677–683.

[7] Denney TS Jr, Prince JL. 3D displacement field reconstruction on an irregular domain from planar tagged cardiac MR images. In: Proc IEEE Workshop on Non-rigid and Articulate Motion, Austin, TX; 1994.

[8] Osman, N. F. , Sampath, S., Atalar, E., Prince J. L., "Imaging longitudinal cardiac strain on short-axis images using strain-encoding MRI," Magn Reson Med 46, 324–334(2001).

[9] Osman, N. F., Prince, J. L., "Visualizing myocardial function using HARP MRI," Phys Med Rio 45, 1665– 1682(2000).

[10] Osman, N. F., Kerwin, W. S., McVeigh, E. R., Prince, J. L., "Cardiac motion tracking using CINE harmonic phase (HARP) magnetic resonance imaging" MRM 42,1048–1060(1999).

[11] Pan, L., Stuber, M., Kraitchman, D. L., and Osman N. F., "Real-time imaging of regional myocardial function using fast-SENC" MRM 55, 386-395(2006).

[12] Abdallah G. Motaal, Nael F. Osman, "Strain Correction in Interleaved Strain- Encoded (SENC) Cardiac MR". Proc SPIE Medical Imaging, Biomedical Applications in Molecular, Structural, and Functional Imaging; San Diego, CA; 2010